



Impact of magnetic, atomic and microstructural ordering on the magnetocaloric performance of powdered NiCoMnSn metamagnetic shape memory ribbons

B. Rodríguez-Crespo^{a,1}, N.A. Río-López^{a,1}, P. Lázpita^{a,b}, S. Ceballos^a, M. Ríos^a, D. Domenech^a, J.A. Rodríguez-Velamazán^c, J. López-García^{d,e}, V. Chernenko^{a,b,f}, J.M. Porro^{a,f,*}, D. Salazar^{a,*}

^a BCMaterials, Basque Center for Materials, Applications and Nanostructures, UPV/EHU Science Park, 48940 Leioa, Spain

^b Department of Electricity and Electronics, Faculty of Science and Technology, University of the Basque Country, 48080 Bilbao, Spain

^c Institute Laue-Langevin, 71 Avenue Des Martyrs, CS 20156, 38042 GRENOBLE Cedex 9, France

^d Department of Physics, Faculty of Science, University of Oviedo 33007, Spain

^e Instituto Universitario de Tecnología Industrial de Asturias, Universidad de Oviedo, Gijón 33203, Spain

^f Ikerbasque, Basque Foundation for Science, 48009 Bilbao, Spain

ARTICLE INFO

Keywords:

Metamagnetic shape memory alloys
Inverse magnetocaloric effect
Neutron powder diffraction
Magnetic ordering
Atomic ordering

ABSTRACT

Co-doped NiMnSn Heusler-type metamagnetic shape memory alloys (MMSMAs) are promising materials for the next-generation solid-state refrigeration systems due to their excellent magnetocaloric performance around the martensitic transformation, which is easily tuneable by slight changes in the alloy composition. An improvement in the thermal efficiency of active magnetic regenerator devices, a key element in magnetocaloric cooling systems, arises by obtaining powdered magnetocaloric alloys that meet technical requirements for their implementation as a feedstock material in the additive manufacturing of 3D-printed heat exchangers. In the present work, powders of Mn-rich NiCoMnSn Heusler-type MMSMAs were obtained from their ribbon form avoiding or minimizing residual stresses, the number of defects and disorder in the crystal lattice and microstructure. Since atomic order and crystallographic structure are crucial in the transformation and magnetic properties of these alloys, a complementary structural analysis of the powders after different heat treatments was performed by powder neutron diffraction. The results show that the cubic austenitic phase of the non-heat-treated melt-spun powder exhibits a highly stressed structure, which leads to an incomplete martensitic transformation and, therefore, to the coexistence of martensitic and austenitic phases at low temperatures. The magnetic structure of the austenite phase was also determined by neutron powder diffraction, obtaining a ferromagnetic coupling between 4a and 4b Wyckoff positions in the samples analysed. It was found that a heat treatment facilitates the martensitic transformation and enables the formation of a pure martensitic phase.

The observed changes in the magnetocaloric performance of the powders have been understood in terms of the differently stressed structures and their impact on the martensitic transformation. A fully completed structural transformation leads to a significant increase of the magnetisation change across the martensitic transformation and, consequently, to high values of both a magnetic field induced isothermal entropy change and refrigeration capacity.

1. Introduction

Heusler-type alloys are widely studied compounds since the discovery of the Cu₂MnAl compound by Fritz Heusler in 1903, which exhibits ferromagnetism although none of its components is ferromagnetically

ordered [1]. These alloys are a class of intermetallic materials with 1:1:1 (Half-Heusler) or 2:1:1 (Heusler) stoichiometry [2]. Specifically, Heusler-type Mn-rich Ni-Mn-based MetaMagnetic Shape Memory Alloys (MMSMAs) represent a set of alloys that exhibit Inverse Magnetocaloric Effect (IMCE), making them of great interest as candidates for solid-state

* Corresponding authors.

E-mail addresses: jm.porro@bcmaterials.net (J.M. Porro), daniel.salazar@bcmaterials.net (D. Salazar).

¹ Equally contributing authors.

<https://doi.org/10.1016/j.matdes.2024.113279>

Received 20 June 2024; Received in revised form 17 August 2024; Accepted 26 August 2024

Available online 28 August 2024

0264-1275/© 2024 The Authors. Published by Elsevier Ltd. This is an open access article under the CC BY license (<http://creativecommons.org/licenses/by/4.0/>).

refrigeration. MMSMAs undergo a first-order phase transformation from a high temperature cubic ferromagnetic austenitic phase to a lower symmetry weak magnetic martensitic phase at a lower temperature, called Martensitic Transformation (MT), which involves a significant change in its magnetic state [3]. Because of the strong magneto-structural coupling [4], the MT in these alloys can be manipulated by an external field [5-7], giving rise to a giant IMCE, which justifies worldwide efforts in the development of cheap, rare-earth-free, non-toxic MCE materials.

The phase stability, the structural and magnetic properties of the aforementioned Ni-Mn-X (X=In, Sn, Sb, Ga, ...) Heusler alloys, non-doped or doped with other elements, have been widely studied theoretically and experimentally, showing that it is possible to handle the magnetic exchange interactions in both the low-temperature martensite and the high-temperature austenite phases, which allows a precise control over the magnetocaloric effect that they present [8-18]. Several previous works have investigated the crystal structures of Ni-Mn-based alloys by means of X-ray or neutron diffraction, concluding that the stoichiometric Heusler alloys present a cubic $L2_1$ -ordered structure with four interpenetrating face centered cubic (fcc) sublattices [19-23].

In an ideal ordered case, the (0, 0, 0) (4a) and $\left(\frac{1}{2}, \frac{1}{2}, \frac{1}{2}\right)$ (4b) sites are taken by Mn and X atoms, respectively, leaving the remaining equivalent $\left(\frac{1}{4}, \frac{1}{4}, \frac{1}{4}\right)$ and $\left(\frac{3}{4}, \frac{3}{4}, \frac{3}{4}\right)$ (8c) sites for Ni atoms [24].

In off-stoichiometric alloys, some amount of Ni, Mn and X atoms may occupy the atomic sites randomly, giving rise to some degree of disorder in the crystal structure [25].

A particular type of these Ni-Mn-based Heusler alloys, Co-doped Ni-Mn-Sn alloys, are of great interest since they have been reported to exhibit MT near room temperature [26]. Umetsu *et al.* showed that a Co-doped Ni-Mn-Sn alloy presents a cubic $L2_1$ austenite at room temperature [27] with space group of $Fm-3m$ (Cu_2MnAl prototype). It was in line with the previous study on Mn-based $Ni_{40}Mn_{42.5}Co_8Sn_{9.5}$ alloy at room temperature [28]. Moreover, Umetsu *et al.* concluded that in the non-doped Ni-Mn-Sn alloy the Mn moments on 4a and 4b sites are coupled antiferromagnetically, whereas in their Co-doped analogues these are coupled ferromagnetically, concluding that the ferromagnetic enhancement was due to the change in magnetic structure by substitution of Ni for Co [27].

In general, Heusler-type MMSMAs are very sensitive to the element content and the crystal structure variations in terms of their martensitic phase transformation temperature [29,30], Curie temperature [31] and saturation magnetisation [32,33]. Post-annealing processing and different cooling rates can produce a strong influence on the magnetic properties [34] through possible changes in the atomic ordering ($B2$ and/or $L2_1$) and/or due to the possible appearance of secondary phases and/or residual martensitic phases. Hence, the parameters of material processing may lead to a degradation or an improvement of the magnetic properties of these compounds [28].

Among the wide range of manufacturing techniques used to obtain magnetocaloric Heusler alloys, melt-spinning outstands. This advanced technique allows to obtain ready-shaped magnetocaloric materials with high surface/volume ratio suitable for their implementation in active magnetic regenerators. Owing to a high solidification rate of the melt (about $10^6 \text{ K}\cdot\text{s}^{-1}$), this technique can modify the physical characteristics of the melt-spun alloys. Their atomic order and crystalline structure are important ingredients for the performance of the aforementioned functionalities of Ni-Mn-based Heusler alloys. Therefore, a deep understanding of the crystal structure of these alloys is required in order to exploit all their functionalities towards the optimisation of their properties [35,36].

Powdered magnetocaloric alloys must meet several technical requirements for their implementation as a feedstock material in the additive manufacturing of 3D-printed active magnetic regenerators with

enhanced thermal transfer, a key element in next-generation solid-state refrigeration systems. Obtaining a functional Heusler-type MMSMA-based magnetocaloric powder does not represent a simple procedure; some experimental issues must be first overcome during the synthesis [28,37].

In the present work we have studied the effect of the multiple ordering on the magnetocaloric performance of two MCE powders with compositions close to the nominal $Ni_{43}Mn_{39}Co_7Sn_{11}$ Heusler-type MMSMA. These powders were obtained from the mechanical grinding of melt-spun ribbons. Differential scanning calorimetry (DSC), powder neutron diffraction and magnetic characterisation techniques were used for a complete characterisation of their properties, and the magnetocaloric effect was calculated based on the obtained thermomagnetsation data. Also, the influence of specific heat-treatments on the martensitic transformation of magnetocaloric powders with similar compositions was evaluated from the DSC ramps and the temperature evolution of their magnetisation. A relationship between the magnetic behaviour of the powders and their atomic ordering and magnetic structure was established, the latter one being determined by powder neutron diffraction experiments, in terms of the presence or absence of internal stress in the structure and their atomic and magnetic ordering [38,39]. It was confirmed that the magnetocaloric performance of the studied MMSMA powders directly depends on the magnetic state change that occurs in the course of the structural transformation from the ferromagnetic austenite to the weak magnetic martensitic phase. The impact of the presence of strains on the aforementioned structural transformation and, therefore, on the magnetic field induced entropy change was disclosed as an effect of the uncompleted martensitic transformation and its subsequent presence of austenitic phase at low temperature. The increased magnetisation in the austenite phase for both compositions is attributed to the enhanced ferromagnetic coupling in the octahedral sites of the crystallographic unit cell.

2. Experimental

2.1. Fabrication of Ni-Co-Mn-Sn powders

A polycrystalline master alloy with a nominal composition of $Ni_{43}Co_7Mn_{39}Sn_{11}$ (at.%) was fabricated by induction melting from pure constituent elements (with purity 99.9%+) under an Ar atmosphere in a quartz crucible. Subsequently, two batches of melt-spun ribbons were fabricated in an Edmund-Buhler melt-spinning system under Ar atmosphere by melting the entire bulk piece (~5 g) and then ejecting the molten alloy onto a rotating copper wheel. The parameters employed to prepare the melt-spun ribbons are a 0.75 mm ejection orifice in the quartz crucible and a $30 \text{ m}\cdot\text{s}^{-1}$ linear speed of the copper wheel. The specific choice of these parameters in order to optimize the magnetocaloric performance of the ribbons was discussed elsewhere [28]. The melt-spun ribbons were carefully grinded using an agate mortar and pestle tool. In order to minimize the phase degradation during the grinding process the ribbons were grinded at 77 K, so that they are in their low-symmetry martensitic phase, by using liquid Nitrogen, and then sieved with a 100 μm orifice mesh.

2.2. Heat treatments

Powder processing, such as melt-spinning and grinding processes, can induce some disorder and residual stresses in the crystal structure, producing undesired effects that result in a detriment of their magnetic properties. These factors affect particularly the aforementioned Ni-Mn-X family of MMSMAs and can be reverted by performing appropriate heat treatments of the prepared powder, as it is well-known that a heat treatment can influence the crystal structure, microstructure, surface and internal stresses relaxation, and even lead to a reduction of the defects [3,40,41].

Since the studied powders belong to the family of alloys reported in

Rodríguez-Crespo et al. [28], the same heat treatments were used with the goal of elucidating the role of the atomic order after specific heat treatments in the magnetic and structural properties of the studied alloys. In particular, the following heat treatments have been applied to our alloys:

- (i) HT1: 1173 K for 1 h + ice water quench
- (ii) HT2: 1173 K for 1 h + ice water quench followed by 723 K for 30 min + ice water quench

The second heat treatment at 723 K is directly related to the induction of a specific atomic ordering, resulting in a higher magnetisation jump around the martensitic transformation, by stabilising the L2₁ ordering in the austenite phase. Heat treatments were carried out by sealing the powders in Argon purged quartz ampoules, and placing them in a high temperature furnace (NBD-O1200-50ICR). Heat treatments were followed by quenching the alloys in the ampoules in iced water.

2.3. Characterisation techniques

The alloys composition and their microstructure were studied by a Hitachi TM3000 scanning electron microscope equipped with an energy-dispersive X-ray detector (SEM/EDS). EDS measurements were carried out on several pieces of ribbons using different areas for each piece, averaging the measured compositions in at. %.

The crystal structure was determined by powder neutron diffraction. The experiments were carried out at the D20 instrument of the Institute Laue-Langevin neutron source (Grenoble, France), with a monochromatic neutron beam of $\lambda = 1.54 \text{ \AA}$. High resolution isothermal diffractograms were obtained at 123, 203, 323 and 423 K for the studied powders, corresponding to the weak-magnetic martensite, paramagnetic martensite, ferromagnetic austenite and paramagnetic austenite phases, respectively. From the obtained data, the crystal structure (lattice parameters and atomic order), as well as residual stresses in the aforementioned phases and the magnetic structures, were determined via LeBail and Rietveld refinements, respectively. FullProf suite software was used for the analysis [42].

The magnetic properties of the powdered samples were studied using a Vibrating Sample Magnetometer from MicroSense Inc. (the field and temperature ranges were 0–2 T and 100–500 K, respectively) and a SQUID-VSM magnetometer from Quantum Design Inc. (the magnetic field and temperature ranges were 0–7 T and 5–400 K, respectively). The calorimetric measurements were performed with a DSC instrument (Mettler Toledo 822e) in the temperature range of 220–425 K. The magnetic field-induced entropy changes were calculated from the thermomagnetisation curves obtained at various applied magnetic fields from 0.01 T to 7 T using Maxwell relationships.

3. Results and discussion

3.1. Structural and transformation behaviour of powdered NiCoMnSn MMSMAs

3.1.1. Composition

The composition of the two ribbons from which the studied powders were manufactured was evaluated by EDS, and the results are shown in Table 1. The instrumental uncertainty of the composition determination by EDS analysis is $\pm 0.5 \text{ at. %}$.

Table 1

Compositions (in at.%) of the ribbons from which the studied powders were obtained.

Composition	Ni	Mn	Sn	Co
A1	43.3	39.2	10.1	7.4
A2	43.3	39.8	10.3	6.6

3.1.2. Transformation characteristics

The temperature dependences of the low-field magnetisation, $M(T)$, as well as calorimetric (DSC) curves, presented in Fig. 1 and Fig. 2, respectively, were used to determine the characteristic transformation temperatures and hysteresis of the MT, as well as the Curie temperature of the studied powders. The temperatures were determined using the derivative method for $M(T)$ curves and by identifying the peak position of the maxima and minima on DSC curves. The dependences of the magnetisation and the heat flow observed in both figures infer a strong effect of the different heat treatments on the transformation behaviour of the alloys. In particular, it can be observed that the heat treatments produced shifts of the characteristic structural and magnetic transformation temperatures, as well as reduction of the thermal hysteresis of MT. The martensitic transformations and Curie temperatures were verified by DSC measurements, where the direct and reverse MTs are accompanied by exothermal and endothermal effects, respectively (Fig. 2). The sample A2 presents about twice larger maximum magnetisation value than A1. This can be attributed to the presence of anisotropic effects induced by the fabrication method of powders (crystal texture or shape anisotropy). At high magnetic fields, when the magnetocrystalline anisotropy is overcome by the field, both samples show similar values of the saturation magnetisation.

The characteristic temperatures of the magnetic (T_C) and structural (T_A and T_M) phase transitions, extracted from the $M(T)$ and DSC curves, as well as the entropy change calculated from the calorimetric measurements during heating are summarized in Table 2. The temperatures obtained using the aforementioned two techniques give similar results.

3.1.3. Powder neutron diffraction

Neutron diffraction patterns of the four powders shown in Table 2 have been measured at specific temperatures, namely 123 K, 203 K, 323 K and 423 K, in order to keep track of the temperature evolution of the different structural and magnetic phases present in the alloys. As an example, Fig. 3 shows the pattern-matching LeBail refinement performed for the 423 K and 123 K diffractograms of the A1 HT2 sample. Table 3 summarizes the crystal structural models used to fit the experimental diffraction patterns, depicting information about the space groups and lattice parameters of the four MMSMA powder alloys studied. All the samples present a Fm-3m cubic symmetry in the austenitic phase and a 3M modulated P2/m monoclinic structure in the martensitic one [41], indicating that there are no changes in the crystal symmetry associated with the heat treatments. Nonetheless, a slight increment of the cell parameters (a_a and c_m) for the HT2 alloys is

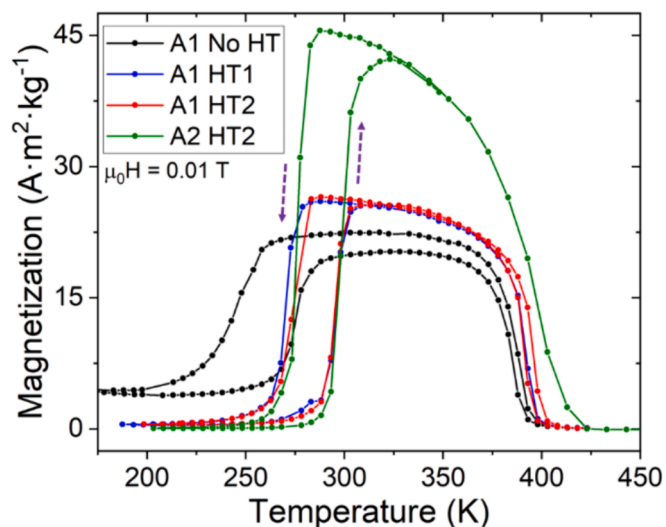


Fig. 1. Magnetisation versus temperature dependences for the heat-treated and non-heat-treated powders at low magnetic field (0.01 T).

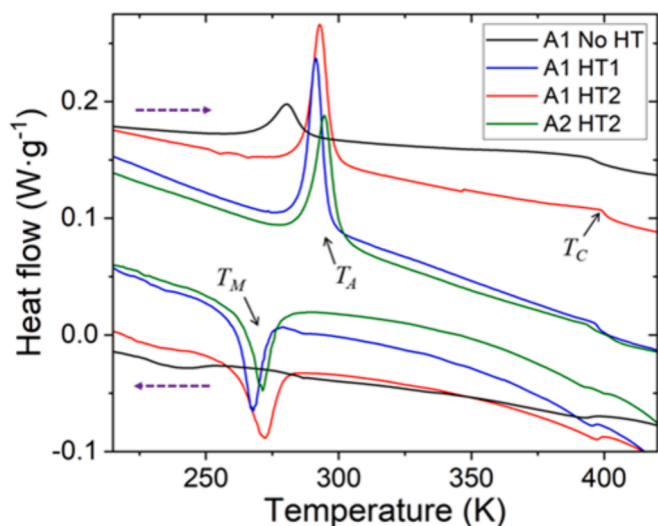


Fig. 2. Differential scanning calorimetry curves for the heat-treated and non-heat-treated powders.

Table 2

Transformation temperatures obtained from the low magnetic field thermomagnetisation curves by the derivative method / and from the positions of the maxima and minima on DSC curves, and the entropy change of the MT.

Powder alloy	T_C , K	T_A , K	T_M , K	ΔS , J·kg ⁻¹ ·K ⁻¹
A1 NoHT	388 / 395	275 / 280	248 / 242	18.1
A1 HT1	393 / 396	296 / 291	270 / 268	47.3
A1 HT2	391 / 398	296 / 293	273 / 272	45.2
A2 HT2	397 / 403	298 / 295	277 / 271	51.5

observed, which can be related to the relaxation of the matrix. In fact, the refinements revealed the existence of internal stresses in the austenite phase of the non-heat-treated sample. The presence of these internal stresses results in an incomplete martensitic transformation during cooling, leading to a coexistence of austenitic and martensitic phases at low temperatures. The presence of internal stresses can be deduced by inspecting the diffractogram peaks corresponding to the cubic austenite phase presented in Fig. 4. A more stressed structure implies a wider peak as it is obvious from this figure. In heat treated samples the internal stresses are relieved which is reflected in narrowing peaks. A significant difference in the peak width at higher angles associated to this phenomenon can also be appreciated. The (331) and (420) peaks, corresponding to B2 and L2₁ ordering, respectively, are shown as the examples of higher angle peaks, whereas the (200) peak is representative of the low angle one. There is no apparent difference between the effect of heat treatments HT1 and HT2 in the internal stresses.

Fig. 5 shows the diffractograms measured at 123 K for the A1 noHT and A1 HT2 samples. There is a clear presence of a residual austenitic phase in the non-heat-treated sample, evidenced by the presence of austenitic peaks in these low temperature diffractograms (marked with a green asterisk), in addition to the expected low symmetry martensitic phase peaks. As previously stated and confirmed from this analysis, the stresses in the non-heat-treated austenite prevent a complete MT, leading to the coexistence of both phases at low temperatures. As a result of heat treatment the stresses must be essentially reduced which favours completing the martensitic transformation.

The atomic orderings in the crystal lattices of the four alloys were determined by Rietveld refinements of the diffractograms obtained at 423 K in the austenite phase of the alloys. The martensitic structure inherits this atomic distribution due to the first order diffusionless character of the martensitic transformation in MMSMAs. Table 4

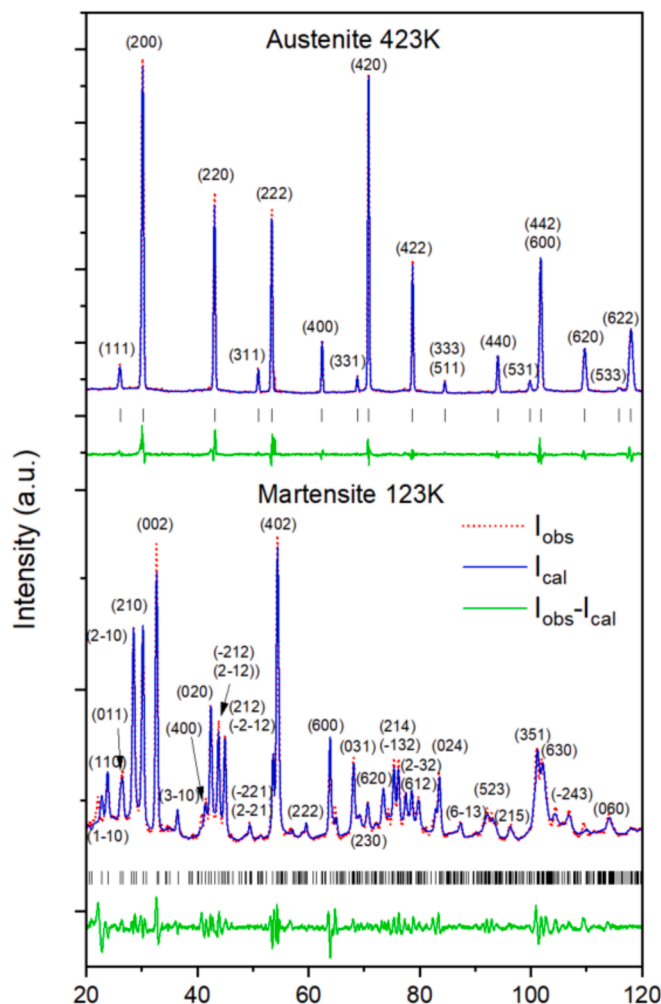


Fig. 3. Le Bail refinements of the neutron diffractograms of the A1 HT2 powder in the austenitic (at 423 K) and martensitic (at 123 K) phases. The experimental data fit the structural models described in Table 3. Red dots represent experimentally measured intensities; blue lines are calculated intensity by Le Bail fittings; green lines, the difference between both intensities; and vertical lines, the position of the indexed crystallographic planes. The Miller indices corresponding to the main indexed planes are also shown. (For interpretation of the references to colour in this figure legend, the reader is referred to the web version of this article.)

Table 3

Structural models, space group and lattice parameters (in Å and °), that fit to the austenite (at 423 K) and martensite (at 123 K) phases in the studied powder alloys.

Powder alloy	T = 423 K		T = 123 K	
	Space group	Lattice	Space group	Lattice
A1 NoHT	F m -3 m	a = 5.97	P 2/m (3 M)	a = 4.40, b = 5.54, c = 4.29, b = 93.17
A1 HT1	F m -3 m	a = 5.97	F m -3 m	a = 5.96
A1 HT2	F m -3 m	a = 5.98	P 2/m (3 M)	a = 4.40, b = 5.53, c = 4.29, b = 93.20
A2 HT2	F m -3 m	a = 5.98	P 2/m (3 M)	a = 4.40, b = 5.53, c = 4.30, b = 93.22
			P 2/m (3 M)	a = 4.40, b = 5.53, c = 4.30, b = 93.04

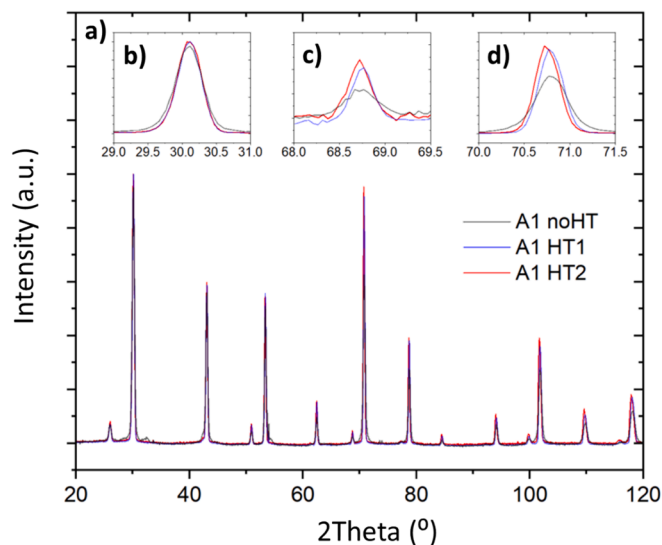


Fig. 4. A) powder neutron diffractograms obtained at 423 K for the A1 noHT (black), A1 HT1 (blue) and A1 HT2 (red) samples, alongside with a zoom image of the b) (200), c) (331) and d) (420) peaks, respectively. For the comparison sake the background in all the patterns were subtracted and the intensity was normalized. (For interpretation of the references to colour in this figure legend, the reader is referred to the web version of this article.)

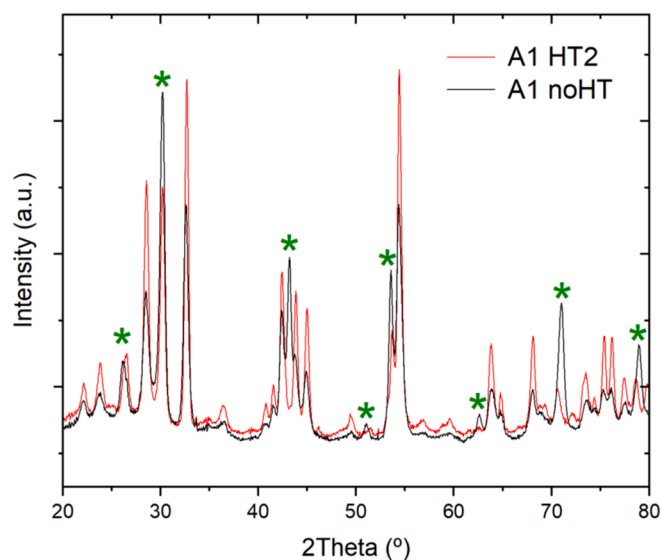


Fig. 5. Powder neutron diffractograms obtained at 123 K for the A1 noHT (black) and A1 HT2 (red) samples. The peaks corresponding to the Fm-3 m austenitic phase are marked with a green asterisk. (For interpretation of the references to colour in this figure legend, the reader is referred to the web version of this article.)

summarises the dependences of the atomic occupancies (in at.%) on the alloy compositions for A1 HT2 and A2 HT2. The results are similar for the non-heat-treated (A1 noHT) and HT1 (A1 HT1) samples, which implies no changes in the atomic ordering related to the manufacturing process. In an ideal situation, the dopant Co atoms should occupy Ni sites only [27,43,44]. In the alloys studied here, there is a lower amount of Co and a higher percentage of Mn in the alloy composition. This leads to a tendency of the Co atoms to occupy all the sites in the unit cell, displacing Mn to Ni. The diffractograms obtained at 423 K for the same-heat-treatment in different-composition samples (A1 and A2) are presented in Fig. 6. Due to the different composition, and, therefore, the different unit cell parameters (see Table 3), the diffraction peaks of each

Table 4

Atomic order at 423 K in the crystal lattices (in at. %) of the paramagnetic austenitic phases (cubic Fm-3 m space group) in the A1 and A2 alloys after HT2. The site occupancy error is approximately 0.2 for all positions.

Powder alloy	Site	Wyckoff position	Ni	Mn	Sn	Co
A1 HT2	Ni - ($\frac{1}{4}$ $\frac{1}{4}$ $\frac{1}{4}$)	8c	43.3	—	—	6.7
	Mn - (0 0 0)	4a	—	25.0	—	—
	Sn - ($\frac{1}{2}$ $\frac{1}{2}$ $\frac{1}{2}$)	4b	—	14.0	10.5	0.5
A2 HT2	Ni - ($\frac{1}{4}$ $\frac{1}{4}$ $\frac{1}{4}$)	8c	43.3	1.5	—	5.2
	Mn - (0 0 0)	4a	—	24.7	—	0.3
	Sn - ($\frac{1}{2}$ $\frac{1}{2}$ $\frac{1}{2}$)	4b	—	13.6	10.3	1.1

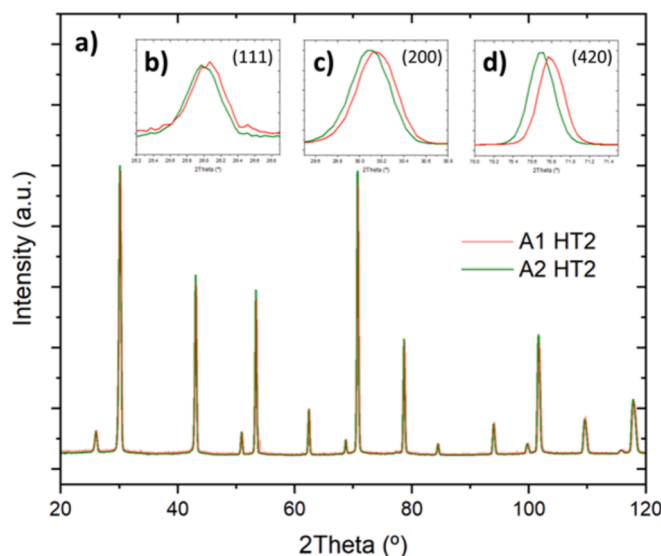


Fig. 6. A) powder neutron diffractograms obtained at 423 K for A1 HT2 (red) and A2 HT2 (green) samples, alongside with a zoom image of the b) (111), c) (200) and d) (420) peaks, respectively. (For interpretation of the references to colour in this figure legend, the reader is referred to the web version of this article.)

alloy are slightly displaced, as evidenced in selected peaks presented as insets of Fig. 6. The differences in the peak heights for each alloy are related to differences in the atomic orderings of the alloys, which are presented in Table 4. Since the same heat treatment was applied to both samples, the residual internal stresses were equally relieved, whereby leading to similar peak widths. Due to A2 HT2 sample composition being higher in manganese than the sample A1 HT2, an increase in magnetisation saturation and T_C should be expected if they are ferromagnetically coupled. A2 alloy presents higher percentage of displaced Mn atoms, that led to higher values of T_C and magnetisation saturation. Therefore, the expected increase in the values is noted below.

These variations in the crystal structures and atomic orders are responsible for the magnetic and structural effects observed in Figs. 1 and 2. Comparing the same-composition different heat-treated samples, one can conclude that a more treated (less stressed) structure favours a completeness of martensitic transformation, increasing MT temperatures and narrowing the thermal hysteresis across the MT. As discussed hereafter, the aforementioned heat treatment-induced changes led to an enhanced IMCE. Regarding the different composition samples after undergoing HT2, the slight increase in the magnetic transition temperature in A2 sample is explained by a competition among the higher amount of Mn on different sites (due to the reduced presence of Co at the Ni positions), which, in contrast to the previous studies performed by Umetsu et al. [27], leads to higher values of T_C .

Fig. 7 shows the Rietveld refinement of the powder neutron

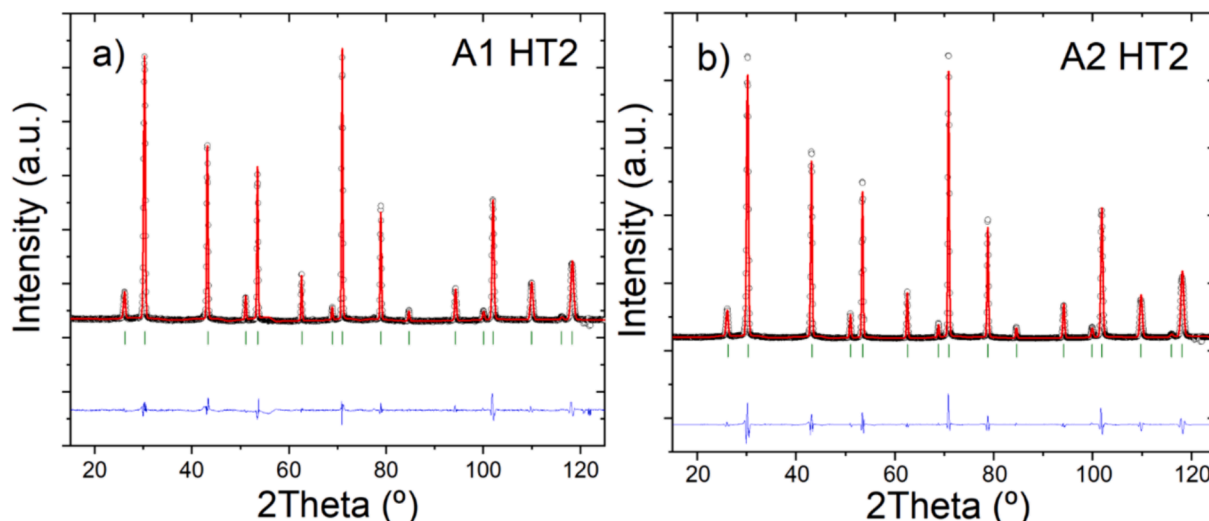


Fig. 7. Powder neutron diffraction patterns in the ferromagnetic austenite state of a) A1 HT2 and b) A2 HT2. Black open circles are the experimental data, red and blue lines represent the calculated and difference patterns, respectively, and green marks indicate the Bragg reflections. (For interpretation of the references to colour in this figure legend, the reader is referred to the web version of this article.)

diffraction data in the magnetically ordered state for samples after being subjected to HT2. The low-temperature patterns show a growth of some nuclear peaks, namely the (200) and the (1 1 1) reflections, upon magnetic ordering. As no purely magnetic peaks appear, it indicates that all samples present a ferromagnetic state. The magnetic Rietveld results (see Fig. 7) reveal the magnetic moment at each Wyckoff position (see Table 5). In the A1 sample, where the Mn atoms are located mainly in the 4a position and the excess goes to 4b site, the magnetic coupling is ferromagnetic with magnetic moments of $2.771(8)\mu_B$ and $0.851(9)\mu_B$, respectively. The presence of Co atoms in the 8c position increases the magnetic interaction between 4a and 4b positions, leading to a ferromagnetic coupling [39,44].

For the A2 sample, as seen in Table 4, Mn and Co atoms are located in all crystallographic positions leading to a disorder $L2_1$ phase. However, the presence of Mn atoms in 8c position leads to a considerable increase of the localized magnetic moment especially in the 4b position in Ni-Mn-In alloys [44,45]. In this case, the presence of Mn atoms in all crystallographic positions increases the magnetic moment on the 4b site by 18 %, resulting in an increase of the total magnetic moment of the alloy and the saturation magnetisation of the sample.

3.2. Magnetocaloric effect

The study of the temperature evolution of the magnetisation of the materials at high magnetic fields is required in order to evaluate their magnetocaloric performance. It is also important to check the temperature evolution of the magnetisation at magnetic fields achievable by the permanent magnets, such as, e.g., 1.5 T [46]. The magnetisation versus temperature ($M(T)$) dependences of the four powders at a field of 1.5 T

Table 5

Magnetic moment determined for 4a, 4b and 8c sites at 323 K in A1 and A2 alloys. Calculated total magnetic moment obtained from neutron diffraction (m_{tot}) and macroscopic magnetisation (m_{sat}) measured in the ferromagnetic austenite.

Powder alloy	Site			Magnetic moment(μ_B /f.u.)	
	4a (μ_B)	4b (μ_B)	8c (μ_B)	m_{tot}	m_{sat}
A1 HT2	2.77 (3)	0.851(9)	0.307*	4.24(4)	4.39(4)
A2 HT2	2.80 (3)	1.04(1)	0.347 (3)	4.53(5)	4.63(5)

*The magnetic moments for Ni and Co are fixed to 0.2 and $1.0 \mu_B$, respectively.

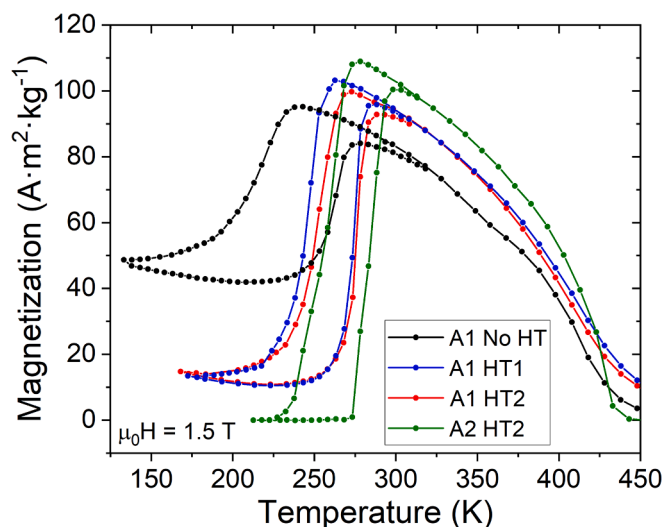


Fig. 8. Magnetisation versus temperature dependences for the studied powders measured under 1.5 T magnetic field.

are shown in Fig. 8. The magnetisation jumps at MT, ΔM , is critically affected by the heat treatments, being doubled for the alloys that underwent a heat treatment with respect to the non-heat-treated one. As a result, a ΔM equal to $110 \text{ Am}^2\text{kg}^{-1}$ was obtained for A2 HT2 powder, which is, to our knowledge, a record-breaking value for any MMSMAs powders yet described in the literature. It should be recalled that the size of ΔM is directly related to the magnetocaloric performance of materials. A direct inspection of the magnetocaloric performance of the alloys can be obtained from the analysis of the $M(T)$ curves measured under different constant magnetic fields up to 5 T, which are presented in Fig. 9. Here, a magnetisation value of $114 \text{ Am}^2\text{kg}^{-1}$ is obtained for A2 HT2.

Following the magnetic field-induced shift of the martensitic transformation in the $M(T)$ curves, phase diagrams of the martensitic and austenitic transformation temperatures as a function of the magnetic field can be obtained. They are shown in Fig. 10. In all cases there is a negative linear dependence of the MT temperatures with increasing magnetic field. The slope of the linear dependence for the heat-treated powders is around $-5.0 \pm 0.2 \text{ K/T}$, whereas the T_M for sample A1

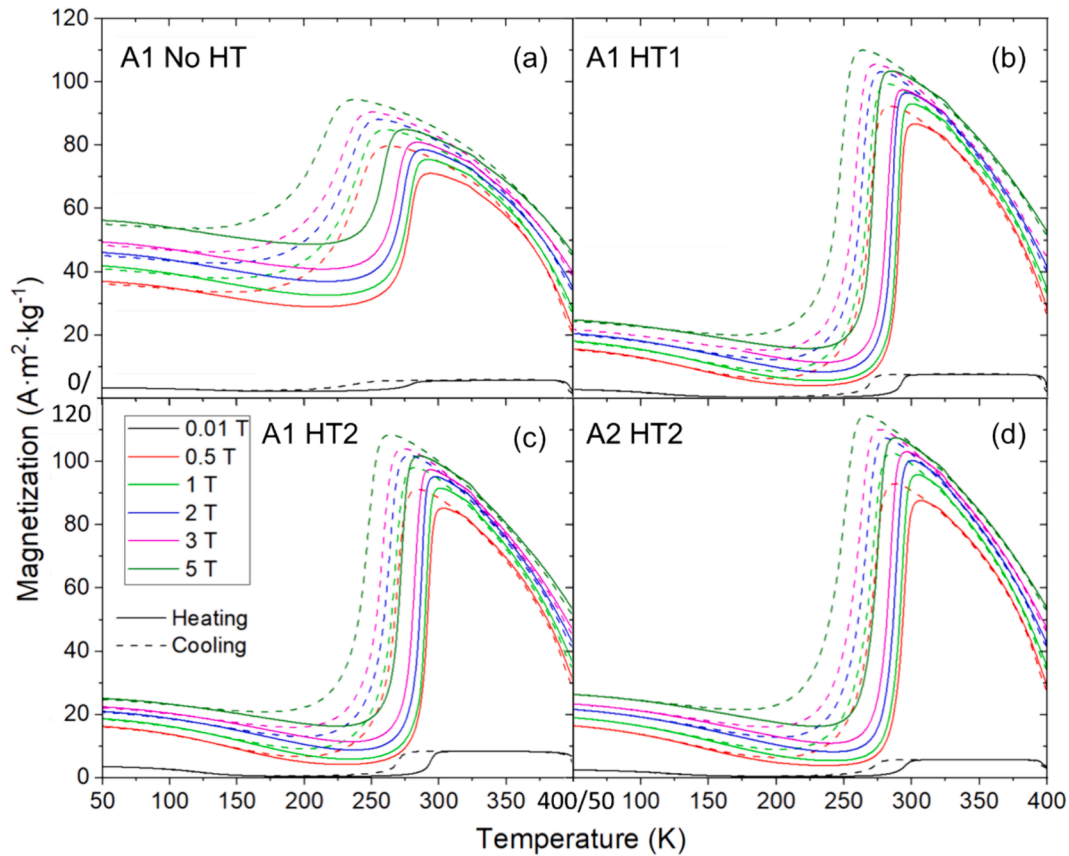


Fig. 9. Thermomagnetisation curves at different magnetic fields for the studied powders.

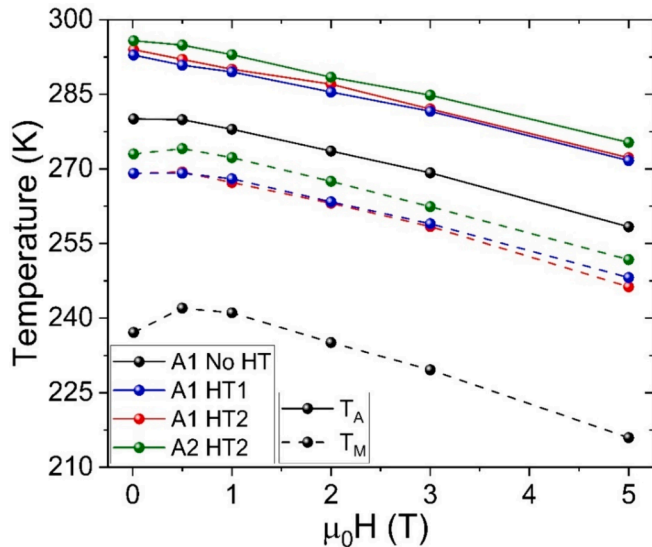


Fig. 10. Phase diagrams of the martensitic transformation temperatures versus magnetic field for all powders.

without heat treatment shows a slope of -6.3 ± 0.1 K/T, both for applied magnetic fields above 0.5 T.

3.2.1. Magnetic field-induced entropy change

The conventional and inverse magnetocaloric effects are characterized by the isothermal entropy change, $\Delta S_m(T, H)$, and the adiabatic temperature change, $\Delta T_{ad}(T, H)$ when a magnetic field is applied or removed in the isothermal or adiabatic conditions, respectively. The

magnetic field induced entropy change can be estimated using Maxwell thermodynamic relationships [47]. From the measured $M(T)$ curves at different magnetic fields (Fig. 9) one can calculate the isothermal entropy change $\Delta S_m(T, H)$ as follows:

$$\Delta S_m(T, H) = S_m(T, H) - S_m(T, 0) = \mu_0 \int_0^H \left(\frac{\partial M(T, H)}{\partial T} \right) dH \quad (1)$$

Fig. 11 shows the $\Delta S_m(T, H)$ plots calculated by using cooling and heating data from Fig. 7 for the four powders studied.

Fig. 11 shows that the heat-treated powders exhibit values of $\Delta S_{m,max} \approx 34 \pm 4$ J·kg⁻¹·K⁻¹ as derived from the analysis of the heating $M(T, H)$ curves at $\mu_0 \Delta H = 5$ T, whereas for the non-heat-treated sample $\Delta S_{m,max} \approx 10$ J·kg⁻¹·K⁻¹. As expected, the maximum magnetic entropy change values obtained at 5 T are below the entropy change values presented in Table 2.

The $\Delta S_{m,max}$ values obtained from the cooling $M(T)$ curves are lower than those obtained from the heating ones due to a more smeared character of the forward MT in comparison with the reverse MT. For example, heating curves at $\mu_0 \Delta H = 2$ T yield $\Delta S_{m,max} \approx 20$ J·kg⁻¹·K⁻¹ for the heat-treated powder A1 HT2; this value falls down to 12 J·kg⁻¹·K⁻¹ for cooling curves at the same field. Noteworthy, the values of $\Delta S_{m,max}$ for the heat treated samples obtained in the present work are comparable to those ones of well-known magnetocaloric materials under similar applied fields; e.g., -18.5 J·kg⁻¹·K⁻¹ for Gd₅(Si₂Ge₂) [48], -19.4 J·kg⁻¹·K⁻¹ for LaFe_{11.4}Si_{1.6} [49], or -25.0 J·kg⁻¹·K⁻¹ for Ni₄₀C₀₈Mn_{42.5}Sn_{9.5} [28].

There is a remarkable difference in the entropy change between the heat-treated and the non-heat-treated powders, as expected from the less abrupt $M(T)$ curve with much smaller ΔM for the non-heat-treated powder in Fig. 9a. For the A1 alloy there is almost no difference in entropy change between HT1 and HT2, as well as between HT2 for both A1

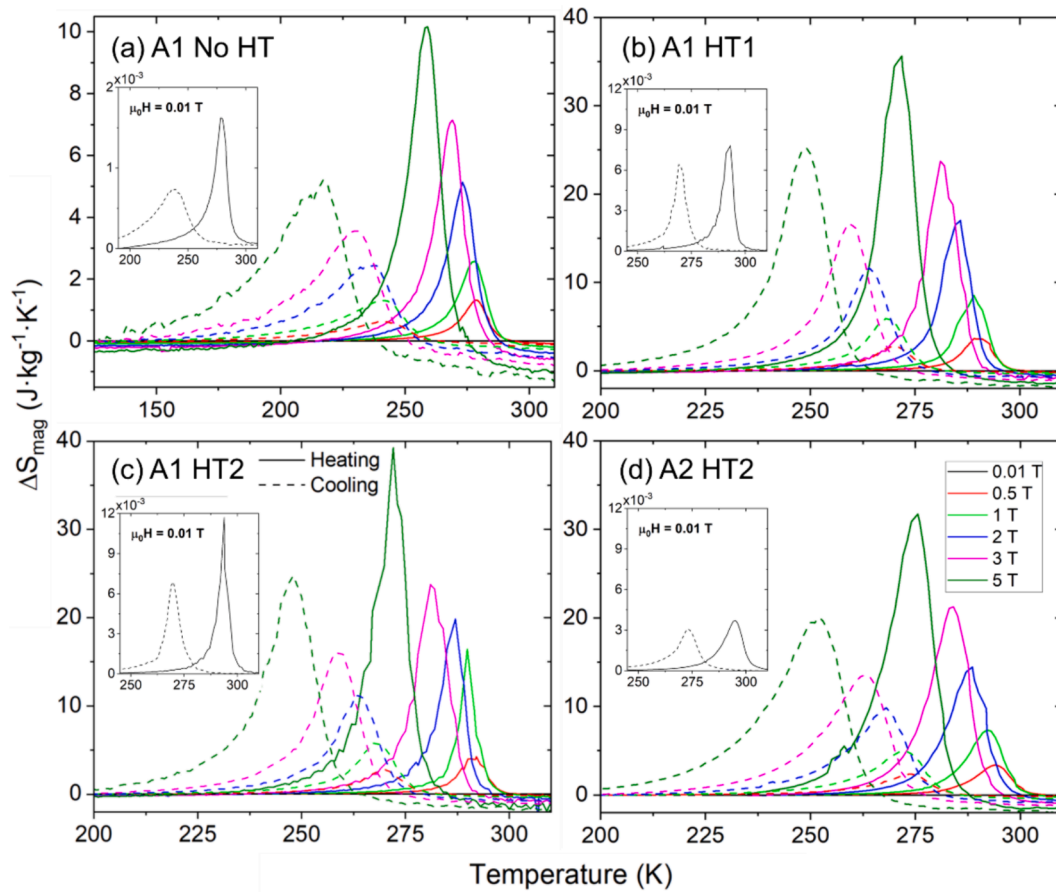


Fig. 11. Magnetic entropy changes at different magnetic fields as a function of temperature for all the studied alloys, derived from cooling/heating $M(T)$ dependences shown in Fig. 7.

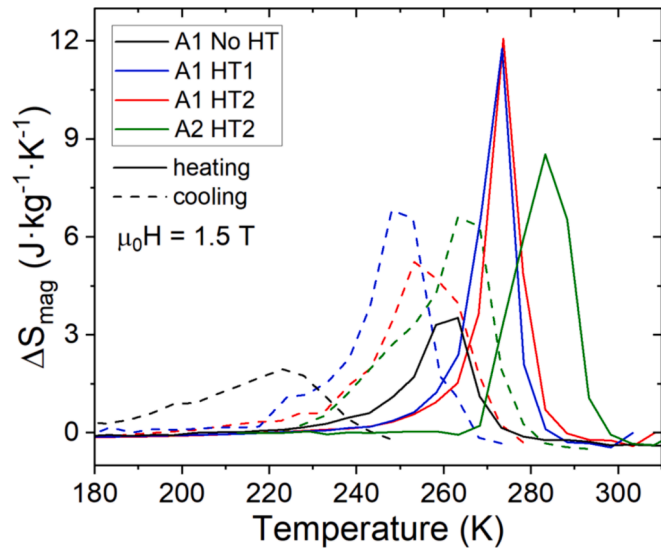


Fig. 12. Magnetic entropy change at 1.5 T for the four powders studied as a function of temperature.

and A2 alloys, with A2 being slightly lower than A1.

Fig. 12 shows a comparison of $\Delta S_m(T)$ dependences of the four samples under an applied field of 1.5 T. As previously mentioned, the difference between the two heat treatments for the A1 powder is negligible in the heating curves whereas in the cooling curves the HT1 sample has slightly higher $\Delta S_{m,max}$ than HT2. Conversely, for the

samples with HT2, the difference in $\Delta S_{m,max}$ between A1 and A2 is negligible during cooling, whereas in the heating curves sample A1 exhibits higher value than A2. For the non-heat-treated alloy $\Delta S_{m,max}$ is about three times smaller than for the rest of the samples.

Fig. 13(a) shows the maxima of the magnetic entropy change ($\Delta S_{m,max}$) as a function of the magnetic field for all samples, whose values increase with the applied field. The non-heat-treated powder shows the lowest increase in $\Delta S_{m,max}$ up to 5 T. In the case of heat-treated powders, although A2 has a higher magnetisation value, A1 has higher $\Delta S_{m,max}$ values than A2 throughout the range. This is observed even for sample A1HT1, possibly due to the slightly more gradual transformation exhibited by A2.

3.2.2. Refrigeration capacity

The refrigeration capacity, RC , is the amount of heat transferred between hot and cold reservoirs in a single refrigeration cycle. It can be calculated by integrating the $\Delta S(T)$ peak at the full width at half maximum (FWHM):

$$RC \approx \int_{T_{cold}}^{T_{hot}} |\Delta S_M(T, H)| dT \quad (2)$$

The value of the integrated area is known as the Gschneidner's calculation [50]. The refrigeration capacity versus magnetic field dependences for cooling and heating ramps, calculated by Eq.(2) using the data from Fig. 11, are shown in Fig. 13(b). The results depicted there demonstrate that $RC(H)$ dependences are affected by the heat treatments, where one can see that the refrigerant capacity is minimal for the non-heat-treated sample and increases with the heat treatments. Note that although the A2 HT2 powder has a slightly smaller maximum

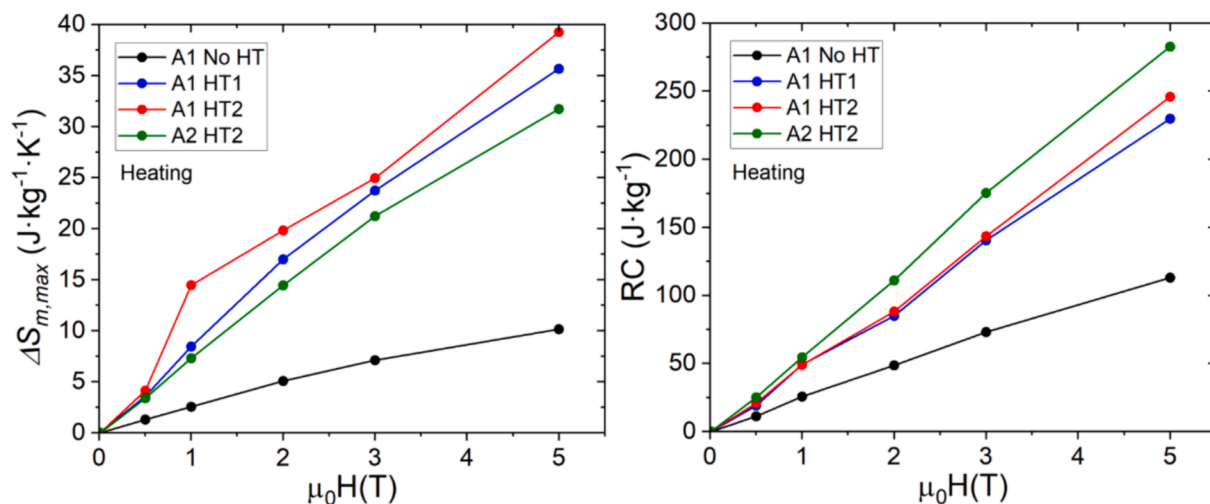


Fig. 13. Refrigeration capacity as a function of the applied magnetic field for cooling (left) and heating (right) ramps for all the alloys studied.

entropy change than A1 HT2, it has the largest refrigeration capacity due to a broader entropy peak.

3.3. Discussion

The results of the thermal, structural and magnetic properties of four powdered MMSMAs ribbons unveiled a crucial role of the heat treatments in their properties. The analysis of these results has evidenced a remarkable improvement of the magnetocaloric performance and refrigeration capacity of the powders when comparing the as-received and heat-treated samples, which is of great importance for their implementation in future solid-state refrigeration devices based on the magnetocaloric effect.

Neutron powder diffraction revealed the changes in the crystal structures of both the austenite and martensite phases induced by heat treatments. In particular, the austenite phase of the non-heat-treated powder exhibited a presence of internal stresses, which relaxed upon the application of both intermediate and complete heat treatments. The crystal structure of the low-temperature martensite phases is also influenced by the heat treatments. The heat-treated powders exhibited a 3 M modulated P2/m monoclinic structure, whereas the coexistence of two crystallographic phases, the expected monoclinic martensite and a residual cubic austenitic phase, was observed for the non-heat-treated sample. Due to the magnetisation jump associated to the martensitic transformation, key for the magnetic field induced isothermal entropy changes, the favoured and completed martensitic transformation arising from the heat-treated samples results in an enhanced magnetocaloric performance. As a direct consequence of these findings, it can be said that heat treatments lead to a crucial improvement of the magnetocaloric performance of the alloys and, hence, to higher refrigeration capacities when compared to the non-heat-treated one.

A mechanism controlling the composition-induced changes in the magnetic properties and structures of powders was disclosed by the analysis of the atomic ordering of the crystal phases of the alloys. It was found that in the A2 alloy the Co atoms tend to occupy all the sites in the unit cell, displacing Mn atoms to Ni sites, whereby increasing the disorder in the unit cell. On the other hand, in the A1 alloy Co atoms tend to be distributed exclusively between Ni and Sn sites, allowing Mn atoms go to their own sites. The presence of Mn and Co in all crystallographic position tends to increase the magnetic interaction between 4a and 4b sites, resulting in an increase of the local magnetic moment of the 4b site that has a ferromagnetic coupling with 4a and 8c sites. This ferromagnetic coupling produces an increase of the total magnetic moment and in the magnetisation of the austenite phase. The increase in magnetisation and T_C value expected in A2 HT2 sample compared to A1 HT1 sample

due to the higher content in manganese is appreciated, due to the higher percentage of displaced Mn atoms interacting ferromagnetically.

4. Conclusions

In the present work we have incorporated a technologically simple method of preparation and heat treatment of the Heusler-type magnetocaloric $Ni_{43}Co_7Mn_{39}Sn_{11}$ (at.%) powders through intermediate stage of obtaining melt-spun ribbons from the master bulk alloy. This method allowed minimizing the content of residual stresses, defects or segregations in the material alongside getting micro-sized grain structure suitable for easy disintegration into powder. The transformation behaviour, crystal structure, magnetic and magnetocaloric properties of the powder samples as a function of the heat treatment regime were systematically studied by DSC, neutron powder diffraction and magnetic measurements, respectively.

Analysis of the atomic site occupancies revealed an enhanced amount of Mn atoms on the Sn sites while Co atoms tended to occupy all unit cell sites in the A2 alloy, increasing unit cell disorder due to displacement of Mn atoms to Ni sites. As for the A1 alloy, the Co atoms moved to the Ni sites, whereby the Mn proper sites become more populated by Mn, in addition to being displaced from the Sn sites. Even though, these rearrangements resulted in a decrease of the displaced Mn atoms and the ferromagnetic coupling remains in the alloy. The expected increase in the magnetisation saturation and T_C comparing A2 to A1, due to the higher content in Mn associated with the composition, was promoted by the higher presence of ferromagnetic interactions.

The non-heat-treated powder obtained from as-received melt-spun ribbon showed an essential presence of residual internal stresses. The heat treatment at 1173 K, usually carried out to improve homogeneity and maintaining the desired phases in MMSMAs, was enough to relieve the presence of those internal stresses. No stresses difference was found with further annealing at 723 K. Heat treatment facilitated the changes in the structural state of the low temperature phase, from the 3 M modulated monoclinic crystal structure for the heat-treated powders to the coexistence of this martensite with residual cubic austenitic phase at 123 K for the non-heat-treated sample. The completed martensitic transformation in the heat-treated samples resulted in the enhancement of both the saturation magnetisation of austenite and its jump at MT. Therefore, the heat-treated NiCoMnSn powders exhibited large values of magnetic field induced isothermal entropy change as well as a high refrigeration capacity.

The key results and main findings of this work are summarised as follow:

The magnetic, atomic and microstructural order, as well as the

martensitic transformation or magnetic transition temperatures, are largely affected by the heat treatments and composition variations in each sample.

The magnetocaloric performance of the studied alloys is strongly related to atomic, magnetic and microstructural ordering, which is also driven by the formation kinetics of the L₂₁ austenite phase, ferromagnetic interactions influenced by atomic occupancy, and the residual stress present in the samples.

A record magnetisation change of 110 Am²kg⁻¹ was obtained around the martensitic transformation at low applied field (1.5 T).

CRedit authorship contribution statement

B. Rodríguez-Crespo: Writing – original draft, Investigation, Formal analysis, Data curation. **N.A. Río-López:** Data curation, Methodology. **P. Lázpita:** Supervision, Investigation, Data curation. **S. Ceballos:** Investigation, Data curation. **M. Ríos:** Visualization, Methodology, Formal analysis. **D. Domenech:** Resources, Formal analysis. **J.A. Rodríguez-Velamazán:** Supervision, Resources. **J. López-García:** Formal analysis, Data curation. **V. Chernenko:** Writing – review & editing, Validation, Project administration. **J.M. Porro:** Writing – review & editing, Supervision, Funding acquisition. **D. Salazar:** Writing – review & editing, Supervision, Funding acquisition, Conceptualization.

Declaration of competing interest

The authors declare the following financial interests/personal relationships which may be considered as potential competing interests: Jose Maria Porro and Daniel Salazar report financial support was provided by Spanish Ministry of Science and Innovation. Natalia Rio-Lopez and Mariana Rios report financial support was provided by Basque Government.

Data availability

Data will be made available on request.

Acknowledgements

The financial support from the Basque Government - Department of Education [project IT1479-22] – Department of Economic Development, Sustainability and Environment [KK-2024/00048 (BISUM-II)] and the grants PID2022-138256NA-C22 and PID2022-138108OB-C33 funded by MCIN/AEI/10.13039/501100011033 are greatly acknowledged. The authors also acknowledge the financial support received from the IKUR Strategy under the collaboration agreement between the Ikerbasque Foundation and BCMaterials on behalf of the Department of Education of the Basque Government. N.A.R.L. and D.D.A acknowledge the funding of Basque Government (Department of Education) under the PREDOC program fellowships no. PREB_2020_1_0002 and PRE-E_2023_1_003, respectively. The authors acknowledge the ILL for beam time allocation through the experiment 5-31-2804 (<https://doi.ill.fr/10.5291/ILL-DATA.5-31-2804>).

References

- [1] P.J. Webster, Heusler alloys, *Contemp. Phys.* 10 (1969) 559–577, <https://doi.org/10.1080/00107516908204800>.
- [2] T. Graf, C. Felser, S.S.P. Parkin, Simple rules for the understanding of Heusler compounds, *Prog. Solid State Chem.* 39 (2011) 1–50, <https://doi.org/10.1016/j.progsolidchem.2011.02.001>.
- [3] Y. Wang, D. Salas, T.C. Duong, B. Medasani, A. Talapatra, Y. Ren, Y.I. Chumlyakov, I. Karaman, R. Arróyave, On the fast kinetics of B₂-L₂ 1 ordering in Ni-Co-Mn-In metamagnetic shape memory alloys, *J. Alloys Compd.* 781 (2019) 479–489, <https://doi.org/10.1016/j.jallcom.2018.12.034>.
- [4] P.J. Webster, K.R.A. Ziebeck, S.L. Town, M.S. Peak, Magnetic order and phase transformation in Ni₂MnGa, *Philos. Mag. B* 49 (1984) 295–310.
- [5] K. Ullakko, J.K. Huang, C. Kantner, R.C.O. Handley, Large magnetic-field-induced strains in Ni₂MnGa single crystals large magnetic-field-induced strains in Ni₂MnGa single crystals, *Appl. Phys. Lett.* 69 (2013) 1966–1998.
- [6] R.Y. Umetsu, W. Ito, K. Ito, K. Koyama, A. Fujita, K. Oikawa, T. Kanomata, R. Kainuma, K. Ishida, Anomaly in entropy change between parent and Martensite phases in the Ni₅₀Mn₃₄In₁₆ Heusler alloy, *Scr. Mater.* 60 (2009) 25–28, <https://doi.org/10.1016/j.scriptamat.2008.08.022>.
- [7] J.A. Monroe, I. Karaman, B. Basaran, W. Ito, R.Y. Umetsu, R. Kainuma, K. Koyama, Y.I. Chumlyakov, Direct measurement of large reversible magnetic-field-induced strain in Ni-Co-Mn-In metamagnetic shape memory alloys, *Acta Mater.* 60 (2012) 6883–6891, <https://doi.org/10.1016/j.actamat.2012.07.040>.
- [8] D.Y. Cong, S. Roth, L. Schultz, Magnetic properties and structural transformations in Ni-Co-Mn-Sn multifunctional alloys, *Acta Mater.* 60 (2012) 5335–5351, <https://doi.org/10.1016/j.actamat.2012.06.034>.
- [9] J. Liu, N. Scheerbaum, S. Kauffmann-Weiss, O. Gutfleisch, NiMn-based alloys and composites for magnetically controlled dampers and actuators, *Adv. Eng. Mater.* 14 (2012) 653–667, <https://doi.org/10.1002/adem.201200038>.
- [10] V. Sokolovskiy, A. Grünebohm, V. Buchelnikov, P. Entel, Ab initio and monte carlo approaches for the magnetocaloric effect in Co- and In-doped Ni-Mn-Ga Heusler alloys, *Entropy* 16 (2014) 4992–5019, <https://doi.org/10.3390/e16094992>.
- [11] H.B. Luo, C.M. Li, Q.M. Hu, S.E. Kulkova, B. Johansson, L. Vitos, R. Yang, First-principles investigations of the five-layer modulated martensitic structure in Ni₂Mn(AlxGa1-x) alloys, *Acta Mater.* 59 (2011) 5938–5945, <https://doi.org/10.1016/j.actamat.2011.06.002>.
- [12] D. Soto, F. Hernández, H. Flores-Zúñiga, X. Moya, L. Mañosa, A. Planes, S. Aksoy, M. Acet, T. Krenke, Phase diagram of Fe-doped Ni-Mn-Ga ferromagnetic shape-memory alloys, *Phys. Rev. B* 77 (2008) 184103, <https://doi.org/10.1103/PhysRevB.77.184103>.
- [13] H.B. Xiao, C.P. Yang, R.L. Wang, V.V. Marchenkov, K. Bärner, Effect of alloying element Al substitution on Ni-Mn-Sn shape memory alloy by first-principle calculations, *J. Appl. Phys.* 112 (2012), <https://doi.org/10.1063/1.4772618>.
- [14] T. Kihara, X. Xu, W. Ito, R. Kainuma, M. Tokunaga, Direct measurements of inverse magnetocaloric effects in metamagnetic shape-memory alloy NiCoMnIn, *Phys. Rev. B - Condens. Matter Mater. Phys.* 90 (2014) 1–6, <https://doi.org/10.1103/PhysRevB.90.214409>.
- [15] V.A. Chernenko, V.A. L'vov, E. Cesari, J.M. Barandiaran, Fundamentals of magnetocaloric effect in magnetic shape memory alloys, *Handb. Magn. Mater.* 28 (2019) 1–45, <https://doi.org/10.1016/BS.HMM.2019.03.001>.
- [16] P. Álvarez-Alonso, C.O. Aguilar-Ortiz, J.P. Camarillo, D. Salazar, H. Flores-Zúñiga, V.A. Chernenko, Adiabatic magnetocaloric effect in Ni₅₀Mn₃₅In₁₅ ribbons, *Appl. Phys. Lett.* 109 (2016) 212402, <https://doi.org/10.1063/1.4968592>.
- [17] J. Yang, Z. Li, B. Yang, H. Yan, D. Cong, X. Zhao, L. Zuo, Effects of Co and Si Codoping on magnetostructural transformation and magnetocaloric effect in Ni-Mn-Sn based alloys, *J. Alloys Compd.* 892 (2022) 162190, <https://doi.org/10.1016/j.jallcom.2021.162190>.
- [18] J. Yang, Z. Li, X. Zhang, B. Yang, H. Yan, D. Cong, X. Zhao, L. Zuo, Manipulation of thermal hysteresis and magnetocaloric effect in the Ni-Co-Mn-In alloys through lattice contraction: effect of Ge substitution for In, *Acta Mater.* 246 (2023) 118694, <https://doi.org/10.1016/j.actamat.2023.118694>.
- [19] P.J. Brown, J. Crangle, T. Kanomata, M. Matsumoto, K.-U. Neumann, B. Ouladdiaf, K. Ziebeck, The crystal structure and phase transitions of the magnetic shape memory compound Ni₂MnGa, *J. Phys. Condens. Matter* 14 (2002) 10159–10171.
- [20] T. Krenke, M. Acet, E. Wassermann, X. Moya, L. Mañosa, A. Planes, Martensitic transitions and the nature of ferromagnetism in the austenitic and martensitic states of Ni-Mn-Sn alloys, *Phys. Rev. B* 72 (2005) 014412, <https://doi.org/10.1103/PhysRevB.72.014412>.
- [21] R.B. Helmholdt, K.H.J. Buschow, Crystallographic and magnetic structure of Ni₂MnSn and NiMn₂Sn, *J. Less-Common Met.* 128 (1987) 167–171.
- [22] A. Ayuela, J. Enkovaara, K. Ullakko, R.M. Nieminen, Structural properties of magnetic Heusler alloys, *J. Phys. Condens. Matter* 11 (1999) 2017–2026, <https://doi.org/10.1088/0953-8984/11/8/014>.
- [23] N.A. Río-López, P. Lázpita, D. Salazar, V.I. Petrenko, F. Plazaola, V. Chernenko, J. M. Porro, Neutron scattering as a powerful tool to investigate magnetic shape memory alloys: a review, *Metals (Basel)* 11 (2021) 829.
- [24] V. Sánchez-Alarcos, V. Recarte, J.I. Pérez-Landazábal, G.J. Cuello, Correlation between atomic order and the characteristics of the structural and magnetic transformations in Ni-Mn-Ga shape memory alloys, *Acta Mater.* 55 (2007) 3883–3889, <https://doi.org/10.1016/j.actamat.2007.03.001>.
- [25] V. Sánchez-Alarcos, J.I. Pérez-Landazábal, V. Recarte, I. Lucia, J. Vélez, J. A. Rodríguez-Velamazán, Effect of high-temperature quenching on the magnetostructural transformations and the long-range atomic order of Ni-Mn-Sn and Ni-Mn-Sb metamagnetic shape memory alloys, *Acta Mater.* 61 (2013) 4676–4682, <https://doi.org/10.1016/J.ACTAMAT.2013.04.040>.
- [26] A. You, M.A.Y. Be, In, I. Metamagnetic Shape Memory Effect in a Polycrystalline Alloy. 2006, 192513, 10–13, doi:10.1063/1.2203211.
- [27] R.Y. Umetsu, A. Sheikh, W. Ito, B. Ouladdiaf, K.R.A. Ziebeck, T. Kanomata, R. Kainuma, The effect of Co substitution on the magnetic properties of the Heusler alloy Ni₅₀Mn₃₃Sn₁₇, *Appl. Phys. Lett.* 98 (2011) 10–13, <https://doi.org/10.1063/1.3548558>.
- [28] B. Rodríguez-Crespo, D. Salazar, S. Lancers-Méndez, V. Chernenko, Development and magnetocaloric properties of Ni(Co)-Mn-Sn printing ink, *J. Alloys Compd.* 917 (2022) 165521, <https://doi.org/10.1016/j.jallcom.2022.165521>.
- [29] S.S. Nambiar, B.R.N. Murthy, S. Sharma, A.A. Prasanna, A.J. Chelvane, Microstructure and mechanical properties of annealed quinary Ni-Mn-Sn-Fe-In Heusler alloy, *Eng. Sci.* 17 (2022) 303–308, <https://doi.org/10.30919/es8d632>.

- [30] S. Esakki Muthu, N.V. Rama Rao, M. Manivel Raja, D.M. Raj Kumar, D. Mohan Radheep, S. Arumugam, Influence of Ni/Mn concentration on the structural, magnetic and magnetocaloric properties in Ni₅₀-XMn_{37+x}Sn₁₃ Heusler alloys, *J. Phys. D Appl. Phys.* 43 (2010), <https://doi.org/10.1088/0022-3727/43/42/425002>.
- [31] V. Zhukova, M. Ipatov, A. Granovsky, A. Zhukov, Magnetic properties of Ni-Mn-In-Co Heusler-type glass-coated microwires, *J. Appl. Phys.* 115 (2014) 10–13, <https://doi.org/10.1063/1.4868919>.
- [32] W. Maziarz, P. Czaja, M.J. Szczerba, L. Lityńska-Dobrzyńska, T. Czeppe, J. Dutkiewicz, Influence of Ni/Mn concentration ratio on microstructure and martensitic transformation in melt spun Ni-Mn-Sn Heusler alloy ribbons, *J. Alloys Compd.* 615 (2015) S173–S177, <https://doi.org/10.1016/j.jallcom.2013.12.164>.
- [33] H. Zheng, W. Wang, S. Xue, Q. Zhai, J. Frenzel, Z. Luo, Composition-dependent crystal structure and martensitic transformation in Heusler Ni-Mn-Sn alloys, *Acta Mater.* 61 (2013) 4648–4656, <https://doi.org/10.1016/j.actamat.2013.04.035>.
- [34] A.S. Kalbfleisch, G. Matthews, P.J. Jacques, On the influence of the cooling rate on the martensitic transformation of Ni-Mn-Sn Heusler alloys, *Scr. Mater.* 114 (2016) 121–124, <https://doi.org/10.1016/j.scriptamat.2015.12.005>.
- [35] C.O. Aguilar-Ortiz, J.P. Camarillo-García, J. Vergara, P. Álvarez-Alonso, D. Salazar, V.A. Chernenko, H. Flores-Zúñiga, Effect of solidification rate on martensitic transformation behavior and adiabatic magnetocaloric effect of Ni₅₀Mn₃₅In₁₅ ribbons, *J. Alloys Compd.* 748 (2018) 464–472, <https://doi.org/10.1016/j.jallcom.2018.03.074>.
- [36] C.O. Aguilar-Ortiz, D. Soto-Parra, P. Avarez-Alonso, P. Lazpita, D. Salazar, P. O. Castillo-Villa, H. Flores-Zuniga, V.A. Chernenko, Influence of Fe doping and magnetic field on martensitic transition in Ni-Mn-Sn melt-spun ribbons, *Acta Mater.* (2016), <https://doi.org/10.1016/j.actamat.2016.01.041>.
- [37] E. Stevens, K. Kimes, D. Salazar, A. Mostafaei, R. Rodriguez, A. Acierno, P. Lázpita, V. Chernenko, M. Chmielus, Mastering a 1.2 K hysteresis for martensitic para-ferromagnetic partial transformation in Ni-Mn(Cu)-Ga magnetocaloric material via binder jet 3D printing, *Addit. Manuf.* 37 (2021) 101560, <https://doi.org/10.1016/J.ADDMA.2020.101560>.
- [38] D.L.R. Khanna, V. Sánchez-Alarcos, V. Recarte, J.I. Pérez-Landazábal, Correlation between particle size and magnetic properties in soft-milled Ni₄₅Co₅Mn₃₄In₁₆ powders, *Intermetallics* 130 (2021) 107076, <https://doi.org/10.1016/j.intermet.2020.107076>.
- [39] J. López-García, V. Sánchez-Alarcos, V. Recarte, J.A. Rodríguez-Velamazán, I. Unzueta, J.A. García, F. Plazaola, P. La Roca, J.I. Pérez-Landazábal, Effect of high-energy ball-milling on the magnetostructural properties of a Ni₄₅Co₅Mn₃₅Sn₁₅ alloy, *J. Alloys Compd.* 858 (2021) 158350, <https://doi.org/10.1016/J.JALLCOM.2020.158350>.
- [40] N.M. Bruno, D. Salas, S. Wang, I.V. Roshchin, R. Santamarta, R. Arroyave, T. Duong, Y.I. Chumlyakov, I. Karaman, On the microstructural origins of martensitic transformation arrest in a NiCoMnIn magnetic shape memory alloy, *Acta Mater.* 142 (2018) 95–106, <https://doi.org/10.1016/j.actamat.2017.08.037>.
- [41] J. López-García, I. Unzueta, V. Sánchez-Alarcos, V. Recarte, J.I. Pérez-Landazábal, J.A. Rodríguez-Velamazán, J.A. García, F. Plazaola, Correlation between defects and magneto-structural properties in Ni-Mn-Sn metamagnetic shape memory alloys, *Intermetallics* 94 (2018) 133–137, <https://doi.org/10.1016/J.INTERMET.2017.12.028>.
- [42] Rodríguez-Carvajal, J. FullProf. 2001.
- [43] V. Sánchez-Alarcos, J. López-García, I. Unzueta, J.I. Pérez-Landazábal, V. Recarte, J.J. Beato-López, J.A. García, F. Plazaola, J.A. Rodríguez-Velamazán, Magnetocaloric effect enhancement driven by intrinsic defects in a Ni₄₅Co₅Mn₃₅Sn₁₅ alloy, *J. Alloys Compd.* 774 (2019) 586–592, <https://doi.org/10.1016/J.JALLCOM.2018.10.016>.
- [44] J. López-García, V. Sánchez-Alarcos, V. Recarte, J.I. Pérez-Landazábal, O. Fabelo, E. Cesari, J.A. Rodríguez-Velamazán, Routes for enhanced magnetism in Ni-Mn-In metamagnetic shape memory alloys, *Scr. Mater.* 167 (2019) 21–25, <https://doi.org/10.1016/J.SCRIPTAMAT.2019.03.025>.
- [45] J. López-García, D.L.R. Khanna, J.L. Sanchez Llamazares, P. Álvarez-Alonso, P. La Roca, V. Recarte, V. Sánchez-Alarcos, J.I. Pérez-Landazábal, J.A. Rodríguez-Velamazán, Magnetic structure analysis of the L21-type austenite in Ni-Mn-In alloys, *Intermetallics* 168 (2024) 108242, <https://doi.org/10.1016/J.INTERMET.2024.108242>.
- [46] T. Gottschall, K.P. Skokov, M. Fries, A. Taubel, I. Radulov, F. Scheibel, D. Benke, S. Riegg, O. Gutfleisch, Making a cool choice: the materials library of magnetic refrigeration, *Adv. Energy Mater.* 9 (2019), <https://doi.org/10.1002/aenm.201901322>.
- [47] V.K. Pecharsky, K.A. Gschneidner, Magnetocaloric effect from indirect measurements: magnetization and heat capacity, *J. Appl. Phys.* 86 (1999) 565–575, <https://doi.org/10.1063/1.370767>.
- [48] V.K. Pecharsky, K.A. Gschneidner, Giant magnetocaloric effect in Gd₅Si₂Ge₂, *Phys. Rev. Lett.* 78 (1997) 4494–4497, <https://doi.org/10.1103/PhysRevLett.78.4494>.
- [49] F.X. Hu, B.G. Shen, J.R. Sun, Z.H. Cheng, G.H. Rao, X.X. Zhang, Influence of negative lattice expansion and metamagnetic transition on magnetic entropy change in the compound LaFe_{11.4}Si_{1.6}, *Appl. Phys. Lett.* 78 (2001) 3675–3677, <https://doi.org/10.1063/1.1375836>.
- [50] K.A. Gschneider. Recent Developments in Magnetic Refrigeration. 1999, 317, 69–76, doi:10.4028/www.scientific.net/MSF.315-317.69..